Supplement of Atmos. Chem. Phys., 18, 14837–14850, 2018
https://doi.org/10.5194/acp-18-14837-2018-supplement

Supplement of

Unprecedented strength of Hadley circulation in 2015–2016 impacts on CO_2 interhemispheric difference

Jorgen S. Frederiksen and Roger J. Francey

Correspondence to: Jorgen S. Frederiksen (jorgen.frederiksen@csiro.au)

1 Pacific and Atlantic westerly ducts

The interhemispheric response to mid-latitude forcing produced by Rossby dispersion through equatorial westerly ducts was documented by Webster and Holton (1982). The zonal winds in the equatorial troposphere are generally easterly but in the upper troposphere the winds may be westerly in the Pacfic duct (centred on 5°N-5°S, 140°W-170°W) or the Atlantic duct (centred on 5°N-5°S, 10°W-40°W) as shown in Fig. 2 of Webster and Chang (1988). As discussed in Francey and Frederiksen (2016, denoted FF16), and shown in Fig. 1S for the period 1992 to 2016 of interest here, the upper-tropospheric zonal wind is strongly correlated with the SOI in the Pacific duct region and anti-correlated in the Atlantic duct region. As the atmospheric circulation changes between La Niña and El Niño conditions the warm ocean temperatures move from the western to eastern Pacific. The upward branch of the Walker circulation follows the warm water and the associated upper-tropospheric westerlies to the east of the uplift successively open the Pacific westerly duct and then the Atlantic westerly duct (Fig. 1 of Webster and Chang 1988). This is the reason for the correlations in our Fig. 1S. The strength (and sign) of the upper-tropospheric zonal velocity in the near-equatorial regions is correlated with corresponding levels in the turbulent kinetic energy which is generated by Rossby wave breaking (Fig. 6 of Frederiksen and Webster 1988). The Pacific duct, u_{duct} of Table 1, is in general the dominant duct as shown in Fig. 2S which depicts the boreal winter (Dec-Feb) upper tropospheric vector wind for 1992-2016.

2 Topographic Rossby waves during February 2015

As noted in the Introduction, the NASA (2016) OCO-2 CO_2 concentration in Fig. 1(a) shows Rossby wave trains over the eastern Pacific and across South America on 17 February 2015. This episode is characteristic of other times of IH Rossby wave propagation during the boreal winter–spring, and particularly February, of 2015. The average 17 to 18 February 2015 streamfunction anomaly, from the thirty year 1981–2010 mean for the same period, is shown in Fig. 3S(a) for the Western Hemisphere (0°W–180°W) between 60°S and 60°N and at the $\sigma = 0.2582$ level. Here $\sigma = \frac{pressure}{surface\ pressure}$ and the corresponding pressure level is circa 260 hPa. We note that the phase lines broadly run from SW to NE between the Southern and Northern Hemispheres but are modulated by some smaller scale features. Moreover the dominant zonal wavenumber $m = 4$.

Indeed there are broad similarities between the streamfunction anomaly in Fig. 3S(a) and the streamfunction for the purely topographic Rossby waves in Figs. 3a and b of Frederiksen and O'Kane (2005). For both the observations considered here and the ensemble of nonlinear simulations and statistical closure calculations the phase lines in the Western Hemisphere run SW to NE and the dominant wavenumber is 4. The dominant wavenumber 4 is also clearly seen in the energy spectra in Fig. 2 of Frederiksen and O'Kane (2005). The SW to NW phase lines of pure topographic Rossby waves are also seen in the linear calculations in Fig. 6 of Frederiksen (1982). In both the linear and nonlinear calculations the topographic Rossby waves are generated by the interaction of westerly winds with a conical mountain located at 30° N (an idealized representation of the massive Himalayan orography) and for a situation where the near equatorial winds are westerly. For the observational results in Fig. 3S(a), the near equatorial winds between 5^{o}S and 5^{o}N are westerly in the Western Hemisphere broadly above 400 hPa and easterly below (not shown).

Figure 3S(b) shows the 300 hPa zonal wind anomaly corresponding to the average 17 to 18 February streamfunction anomaly in Fig. 3S(a). Again the SW to NE phase lines are evident as is the dominant $m = 4$ wavenumber although the presence of smaller scale features associated with disturbances in the storm tracks (typically $m \sim 8 - 12$) is perhaps more evident. In Figs. 4S(a) and 4S(b) we depict latitude pressure cross sections of the zonal wind anomalies for 17 to 18 February averaged between 120^{o}W–140^{o}W and 80^{o}W–100^{o}W respectively. We note that the anomaly is largely equivalent barotropic, as expected for topographic Rossby waves, and, by comparing the two panels, the SW to NW phase tilt is evident throughout the atmosphere. It can also be seen that the propagation across the equator into the Southern Hemisphere occurs primarily in the upper troposphere, particularly between 80^{o}W–100^{o}W where the mean westerly winds are weaker (not shown).

We have also plotted latitude pressure cross sections of anomalies of the vertical velocity in pressure coordinates, $\omega = dp/dt$ where p is pressure, for 17 to 18 February averaged between 120^{o}W–140^{o}W and 80^{o}W–100^{o}W (not shown). These cross sections indicate that there is strong uplift in the Northern Hemisphere between 10^{o}N and 30^{o}N (negative ω) and general descent south of that band to 30^{o}S. The topographic Rossby wave train generated by westerly winds impinging on the Himalayas may interact with a small region of uplift focused over the Andes in Peru (not shown) when it crosses into the Southern Hemisphere. However, in addition it should be noted that the wave train occurs at a time of seasonal minimum in Southern Hemisphere CO_2.

Acknowledgements. We thank Nada Derek and Stacey Osbrough for assistance with the graphics. The dynamics contributions were prepared using data and software from the NOAA/ESRL Physical Sciences Division web site: http://www.esrl.noaa.gov/psd/.

References

1. Francey, R. J., & Frederiksen, J. S.: The 2009–2010 step in atmospheric CO_2 interhemispheric difference, Biogeosciences, 13, 873–885, doi: 10.5194/bg-13-873-2016, 2016.
2. Frederiksen, J. S.: Eastward and westward flows over topography in nonlinear and linear barotropic models, J. Atmos. Sci., 39, 2477–2489, 1982.
3. Frederiksen, J. S., & O'Kane, T. J.: Inhomogeneous closure and statistical mechanics for Rossby wave turbulence over topography, J. Fluid Mech., 539**,** 137–165, 2005.
4. Frederiksen, J. S., & Webster, P. J.: Alternative theories of atmospheric teleconnections and low-frequency fluctuations, Rev. Geophys., 26, 459–494, 1988.

5. Webster, P. J., & Chang, H. R.: Equatorial energy accumulation and emanation regions: Impacts of a zonally varying basic state, J. Atmos. Sci., 45, 803-829, 1988.
6. Webster, P. J., & Chang, H. R.: Equatorial energy accumulation and emanation regions: Impacts of a zonally varying basic state, J. Atmos. Sci., 45, 803-829, 1988.
7. NASA: Following carbon dioxide through the atmosphere, 2016. https://svs.gsfc.nasa.gov/12445

Figure captions

Figure 1S: Correlation over the annual cycle of 1992-2016 upper-tropospheric winds (300 hPa) with the Southern Oscillation Index (SOI).

Figure 2S: Upper-tropospheric (200 hPa) boreal winter (Dec-Feb) vector wind (ms^{-1}) for 1992-2016.

Figure 3S: The average 17 to 18 February 2015 (a) streamfunction anomaly at $\sigma = 0.2582$ in kms^{-1} and (b) zonal wind anomaly at 300 hPa in ms^{-1} where the anomalies are with respect to the thirty year 1981–2010 mean for the same period.

Figure 4S: Latitude pressure (hPa) cross sections of zonal wind anomalies in ms^{-1} for 17 to 18 February 2015 averaged between (a) 120^{o}W–140^{o}W and (b) 80^{o}W–100^{o}W.

Figures

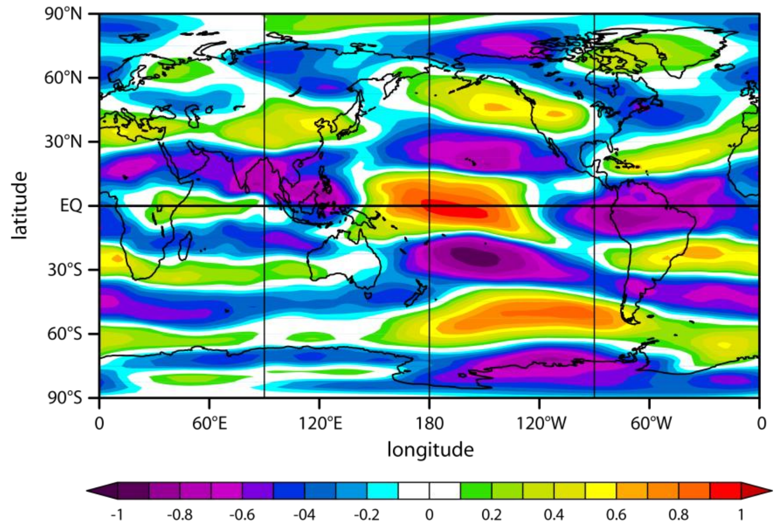

Figure 1S: Correlation over the annual cycle of 1992-2016 upper-tropospheric winds (300 hPa) with the Southern Oscillation Index (SOI).

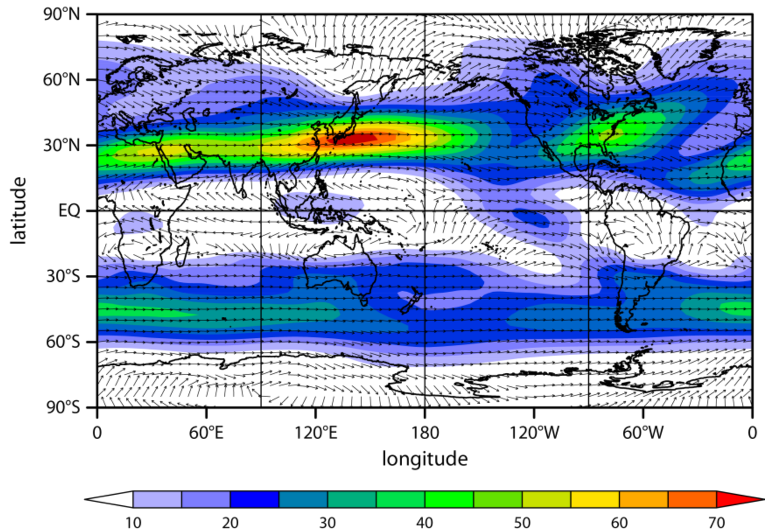

Figure 2S: Upper-tropospheric (200 hPa) boreal winter (Dec-Feb) vector wind (ms^{-1}) for 1992-2016.

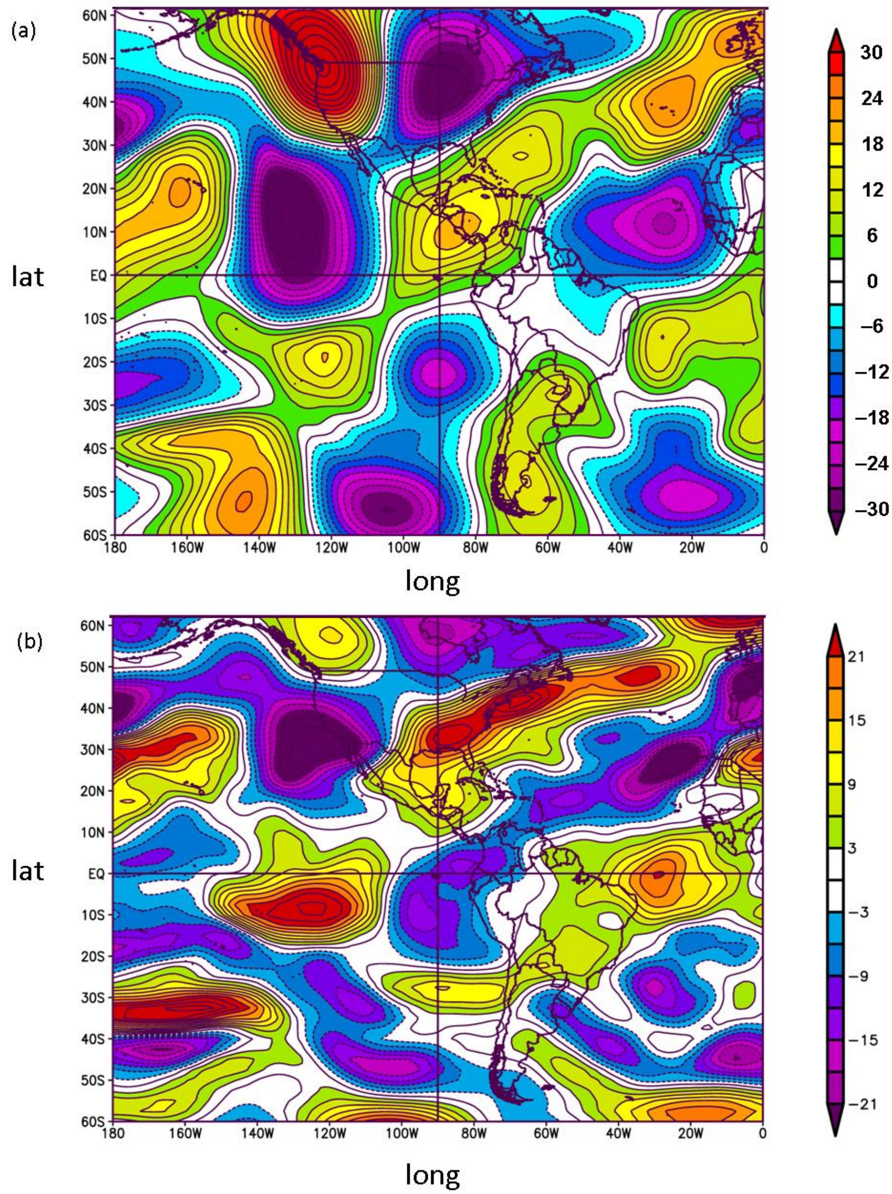

Figure 3S: The average 17 to 18 February 2015 (a) streamfunction anomaly at $\sigma = 0.2582$ in kms^{-1} and (b) zonal wind anomaly at 300 hPa in ms^{-1} where the anomalies are with respect to the thirty year 1981–2010 mean for the same period.

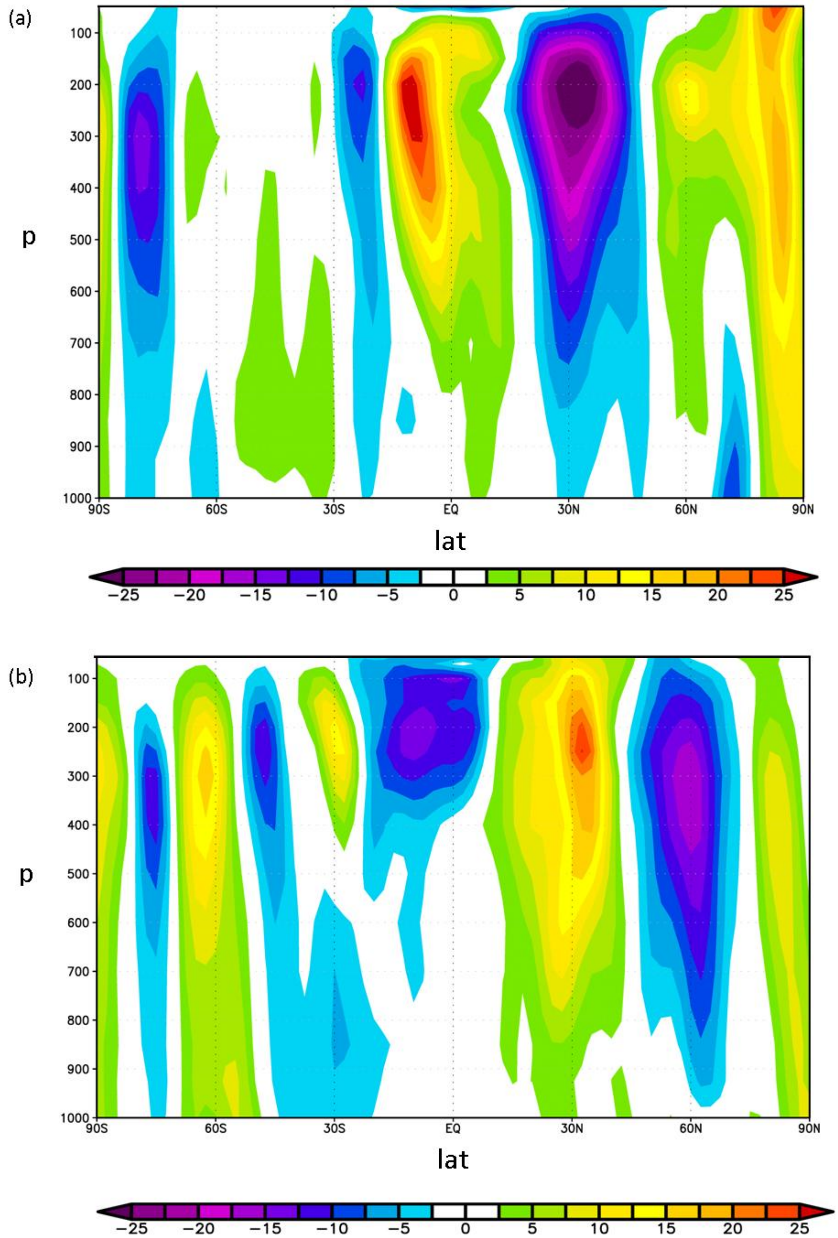

Figure 4S: Latitude pressure (hPa) cross sections of zonal wind anomalies in ms^{-1} for 17 to 18 February 2015 averaged between (a) 120^{o}W–140^{o}W and (b) 80^{o}W–100^{o}W.